Angular momentum distribution in strong-field frustrated tunneling ionization

Jintai Liang (梁锦台)[1], Ruozhou Zhang (张若舟)[1], Xiaomeng Ma (马晓萌)[1], Yueming Zhou (周月明)[1,*], and Peixiang Lu (陆培祥)[1,2]

[1]*School of Physics, Huazhong University of Science and Technology, Wuhan 430074, China*
[2]*Laboratory of Optical Information Technology, Wuhan Institute of Technology, Wuhan 430205, China*
**Corresponding author: zhouymhust@hust.edu.cn*

Received January 7, 2018; accepted February 11, 2018; posted online March 23, 2018

Using the classical-trajectory Monte Carlo model, we have theoretically studied the angular momentum distribution of frustrated tunneling ionization (FTI) of atoms in strong laser fields. Our results show that the angular momentum distribution of the FTI events exhibits a double-hump structure. With this classical model, we back traced the tunneling coordinates, i.e., the tunneling time and initial transverse momentum at tunneling ionization. It is shown that for the events tunneling ionized at the rising edge of the electric field, the final angular momentum exhibits a strong dependence on the initial transverse momentum at tunneling. While for the events ionized at the falling edge, there is a relatively harder recollision between the returning electron and the parent ion, leading to the angular momentum losing the correlation with the initial transverse momentum. Our study suggests that the angular momentum of the FTI events could be manipulated by controlling the initial coordinates of the tunneling ionization.

OCIS codes: 020.2649, 020.4180, 320.7110, 320.7120.
doi: 10.3788/COL201816.040202.

Tunneling ionization is a fundamental process in the intense laser-atom/molecule interactions that occurs when the electric field of the laser pulse is comparable to the Coulomb force. When an atom is subjected to a linearly polarized strong laser pulse, the barrier of the Coulomb potential becomes periodically suppressed, which allows for tunneling of the electrons. After tunneling from an atom, the electron may return back and recollide with the parent ion, leading to various nonlinear phenomena, such as high-order harmonic generation[1–4], high energy above threshold ionization[5–8], and nonsequential double ionization[9–18].

In strong-field tunneling ionization, a large population of neutral atoms surviving in Rydberg states are observed. The underlying mechanism for the creation of these Rydberg states has attracted much interest. It has been shown that in the multiphoton ionization regime[19,20], where the Keldysh parameter $\gamma = \sqrt{I_p/(2U_p)}$[21] is larger than 1, the Rydberg states are created via AC Stark-shifted multiphoton resonant excitation during the laser pulse[22]. For $\gamma < 1$, where the electron ionizes through tunneling, the Rydberg-state neutral atoms have also been observed[23]. It has been demonstrated that the rescattering process is responsible for the formation of these Rydberg atoms in the tunneling regime[23]. This is supported by recent experiments on the ellipticity dependence of the excited neutral atoms yield[23,24]. In this rescattering process, the tunneled electron does not gain enough drift energy from the laser field and it is recaptured by the Coulomb field of the ion when it returns back to the proximity of the parent ion. This is called frustrated tunneling ionization (FTI). This FTI model has been very successful in reproducing the n-distribution (energy) of the Rydberg states and has initiated a variety of studies in laser–atom interactions, such as strong-field acceleration of neutral atoms[25,26] and the survival of Rydberg states in a strong laser field[19,20]. The excited fragmentations in a strong-field dissociation of molecules have also been observed and explained with FTI[27–33].

While the details of FTI, such as the initial tunneling coordinates and the n-distribution of the Rydberg states have been well explored, the angular momentum, which is a very important quantity of Rydberg atoms, has been overlooked in previous studies. The angular momentum of Rydberg states is of great importance for both fundamental and applied physics. For example, the low-angular-momentum Rydberg states were used for optical quantum information manipulations[34–37] and long-lived circular Rydberg levels with high angular momentum are tools in the exploration of cavity quantum electrodynamic effects[38,39]. Thus, it is very important to explore the angular momentum of the Rydberg states in FTI and reveal the relationship between angular momentum and initial tunneling coordinates, and ultimately control the angular momentum distribution of the Rydberg states.

In this work, we theoretically study the angular momentum distribution of the recaptured electrons formed in the FTI process driven by a linearly polarized field using the classical-trajectory Monte Carlo (CTMC) model[40]. We calculate the angular momentum distribution of the recaptured electrons and trace back the initial tunneling coordinates. We reveal the relationship between the initial tunneling coordinates and the final angular momentum of the recaptured electron. Specifically, the final angular

momentum of the electron tunneled on the rising edge of the electric crest of the laser field shows a strong regular dependence on the initial transverse momentum. For the electron tunneled on the falling edge of the electric field crest, there is a relatively harder rescattering by the parent ion, which leads to the final angular momentum of the recaptured electron shifting away from the regular distribution. This process is intuitively revealed by back tracing of the classical trajectories.

In the CTMC model, the FTI process includes two steps: tunneling ionization and classical evolution of the tunneled electron in a combination of the laser field and Coulomb potential of the ion. In the first step, the electron ionizes at the tunnel exit with an initial zero longitudinal momentum and a Gaussian-like transverse momentum distribution. The weight of the trajectory was determined by the tunneling theory[41,42] $\omega = \omega_0(t_0)\omega_\perp(p_\perp)$, where

$$\omega_0(t_0) \propto \left[\frac{2(2I_p)^{3/2}}{|F(t_0)|}\right]^{2/\sqrt{2I_p}-|m|-1} \exp\left[-\frac{2(2I_p)^{3/2}}{3|F(t_0)|}\right], \quad (1)$$

$$\omega_\perp(p_\perp) \propto \exp\left[-p_\perp^2 \frac{\sqrt{2I_p}}{|F(t_0)|}\right]. \quad (2)$$

Here, $F(t_0)$ is the instantaneous electric field of the laser field at tunneling time t_0, $p_\perp$ is the initial transverse momentum, m is the magnetic quantum number, and I_p is the ionization potential. After tunneling, the evolution of the electron's trajectory is determined by Newton's equation of motion (atomic units are used unless stated otherwise)

$$\ddot{\vec{r}}(t) = -\vec{F}(t) - \nabla V(\vec{r}), \quad (3)$$

where $V(r) = -1/r$ is the Coulomb potential between the ion and electron. $F(t) = F_0 \cos^2(\pi t/\tau)\cos(\omega t)\hat{x}$ with $-\tau/2 \le t \le \tau/2$ is the electric field of the laser pulse, which is linearly polarized along the x axis. F_0 is the amplitude of the electric field, $\tau = 10\,T$ is the pulse duration, and T is the optical cycle of the laser field.

In our calculations, we consider a simple case of He where the electron originates from the S state ($m = 0$) and $I_p = 0.9$ (a.u.). The tunneling exit is approximately estimated by $x_0 = -I_p/F(t_0)$. The ensemble is obtained by sampling ten millions of classical trajectories over the ionization time and initial transverse momentum. We examine the energy of the electron when the laser pulse is turned off. The electrons with the final energy $E_f > 0$ stand for the ionized ones. These with $E_f < 0$ correspond to the tunneled electrons recaptured by the ion, which are the FTI events that we will focus on in this study. We estimate the main quantum number n of the bound electron with the Rydberg formula $E_f = -1/(2n^2)$[23]. The angular momentum is calculated as $\vec{L}_f = \vec{r}_f \times \vec{P}_f$. In this study, we focus on the angular momentum distribution of the FTI events.

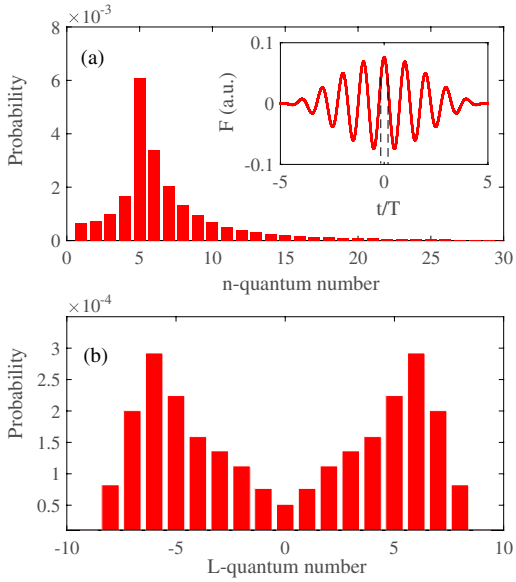

Fig. 1. (a) n distribution and (b) L distribution of the recaptured electrons. The insert in (a) shows the electric field of the laser pulse and the dashed line indicates the tunneling ionization time in our calculations.

In Fig. 1, we show the n-distribution of the FTI events. The insert of Fig. 1(a) shows the electric field of the laser pulse in our calculations, where we only consider the events with tunneling ionization occurring at the peak of the laser pulse, as indicated by the dashed lines. Figure 1(a) exhibits a maximum around $n = 5$ and a long tail extending to higher excited states, with n larger than 30. This result is in agreement with the previous work[23]. We mention that the position of the peak in n-distribution depends on the laser intensity. This explains why in Fig. 1(a) the peak locates at $n = 5$, while in Ref. [23] it is located at $n = 8$ (there a higher laser intensity was used). Figure 1(b) shows the angular momentum distribution of the FTI events, which is the focus of this work. It is shown that the distribution exhibits a double-hump structure.

In order to understand the underlying dynamics for this L-distribution, we take advantage of the CTMC model and trace back to the initial coordinates of the FTI events. In Fig. 2, we show the distribution of the tunneling ionization time and initial transverse momentum of the FTI events. As shown in Fig. 2, those electrons tunneled in the interval $(-0.05\,T, 0.05\,T)$, with a specific range of the initial transverse momentum that can be captured by the parent ion when the laser pulse is turned off. It shows that there is a large nearly continuous area and some irregular structures in the distribution. The continuous part is mainly located before the peak of the electric field while the irregular structure is located around and after the peak of the electric field. According to the classical rescattering model, without taking into account the Coulomb interaction, only the electron tunneling after the peak of the electric field could return back to the parent ion. For the FTI, the Coulomb interaction between the parent ion and the tunneled

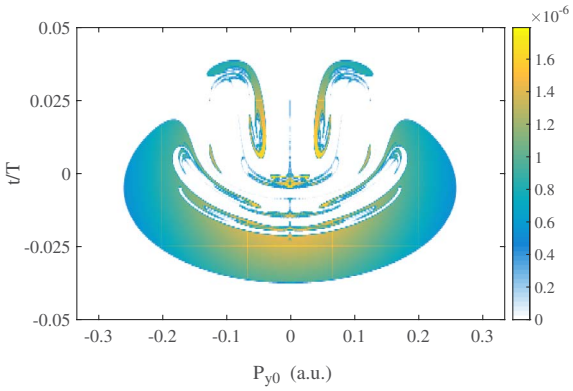

Fig. 2. Probability distribution for FTI in the tunneling coordinate, where t and P_{y0} stand for the tunneling time and the initial transverse momentum at tunneling, respectively. The colorbar on the right represents the recapture probability.

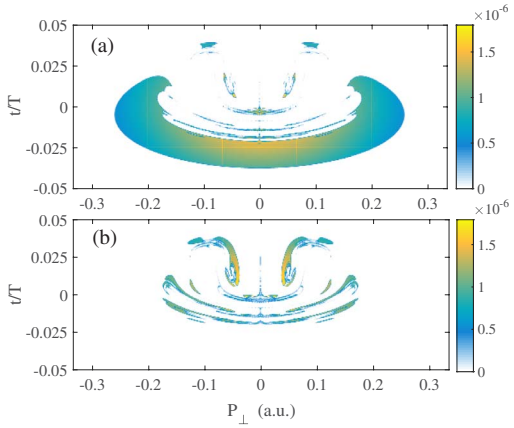

Fig. 4. Tunneling time distribution versus the initial transverse momentum for recaptured electrons. The distribution is divided into two parts. (a) shows the regular part (for the events between the dashed lines in Fig. 3) and (b) shows the irregular part (for the events out of the dashed lines in Fig. 3). The colorbar on the right represents the recapture probability.

electron is very important, which leads to electron tunneling before the peak of electric field that could be recaptured to the orbit of the Rydberg state. The orbits of the Rydberg states sensitively depend on the initial condition of the tunneling electrons. Thus, it can be expected that the angular momentum of these states depends on the tunneling coordinates.

In Fig. 3 we display the final angular momentum distribution versus the initial transverse momentum at tunneling. The region between the dashed lines indicates an almost linear correlation between the final angular momentum and the initial transverse momentum. This part accounts for the dominant amount of FTI events. This correlation implies a general relation between the final angular momentum and the initial velocity at tunneling for FTI. For the small initial transverse momentum $|p_\perp| \leq 0.15$, there are visible distributions out of the region between the dashed lines. The different types of distributions within and out of the region marked by the dashed lines indicate the different mechanisms for the angular momentum.

To shed light on the underlying dynamics, we trace back the tunneling coordinates and divide the FTI events into two parts. Figure 4(a) corresponds to the correlation

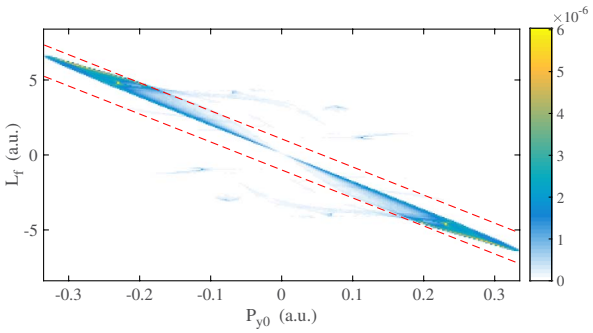

Fig. 3. Final angular momentum distribution versus the initial transverse momentum of the recaptured electrons at tunneling. The colorbar on the right represents the recapture probability.

region between the dashed lines in Fig. 3. This distribution is nearly continuous and is mainly located before the peak of the electric field. According to the simple-man rescattering model[43–46], these electrons cannot return to the parent ion. Thus, it can be expected that no rescattering occurs for these tunneling trajectories. The FTI occurs due to the electron being in the Kepler orbit of the highly excited state after the laser field is turned off. For these trajectories, the final orbits are mainly determined by the initial transverse momentum at tunneling, and thus the angular momentum distribution exhibits a strong correlation with the initial transverse momentum.

For the FTI events in the irregular region out of the dashed lines in Fig. 3, tunneling mainly occurs after the peaks of the electric field, as shown in Fig. 4(b). Additionally, the initial transverse momentum distribution is much less than that in Fig. 4(a). For these trajectories, the electron could return to the parent ion, and relatively harder rescattering occurs. This rescattering changes significantly the shape of the orbit and thus the final angular momentum loses its correlation with the initial transverse momentum.

Thus, we could conclude that irregular behavior for the dependence of the angular momentum distribution on the initial tunneling coordinates is mainly caused by the Coulomb potential during recollision. To explain this issue more intuitively, in Figs. 5(a) and 5(b) we show several illustrative trajectories of the electrons in regular and irregular cases, which stand for the most popular trajectories in both cases. Figure 5(a) represents the trajectories corresponding to the correlation region between the dashed lines in Fig. 3. For these trajectories, the electron tunneling ionization occurs before the peak of the electric field. The different colors stand for the trajectories where the electron ionized with opposite initial transverse momentum at the same tunneling time. For these regular

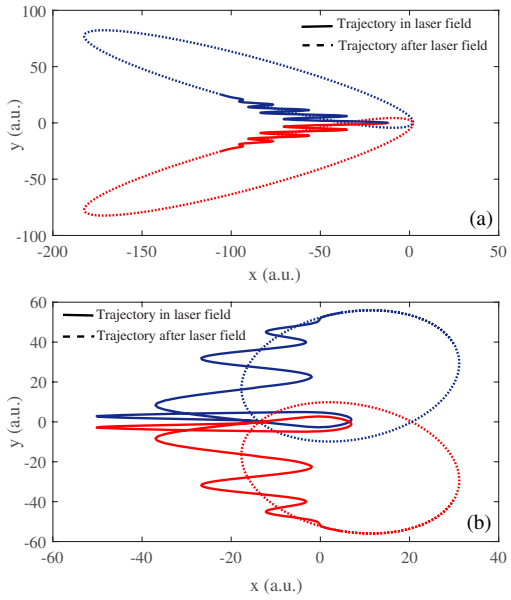

Fig. 5. Typical trajectories for recaptured electrons where the parent ion is located at the origin. (a) and (b) show regular and irregular trajectories, respectively. The solid part represents the trajectory in the combination of the laser field and Coulomb force. The dashed part stands for the trajectories when the laser pulses are over where only Coulomb interaction guides the evolution of the electron. The red and blue curves denote two trajectories ionized at the same instant but with opposite initial transverse momenta.

trajectories, the electron never returns back to the parent ion during the laser pulse. When the laser is turned off, the electron is in the Kepler orbit of some highly excited states. For these trajectories with opposite initial transverse momenta, the electrons finally achieve augular momenta with opposite signs, as shown by the dashed lines. The trajectories shown in Fig. 5(b) correspond to the irregular part of the angular momentum distribution in Fig. 3. These trajectories tunneling ionize after the peak of the electric field and return back to the parent ion about one cycle later. Thus, the Coulomb force is significantly large at this moment, which causes the evolution of angular momentum that does not follow the oscillation of the laser field. So the relationship between the final angular momentum and the initial transverse momentum is much complicated, as shown in Fig. 3.

To show the effect of the Coulomb force during the recollision more clearly, in Fig. 6 we show the force on the electron and the angular momentum evolution during the laser pulse for the irregular case. The solid red curve in Fig. 6(a) stands for the angular momentum of an irregular trajectory while in the dashed black curve we have artificially turned off the Coulomb interaction. In Fig. 6(b), the red curve stands for the total force in the x direction and the blue one is along the y direction. It is clearly shown that there is a sudden change of the force at about $0.8\,T$, when the electron returns to the parent ion. Figure 6(a) compares the evolution of angular momentum of this

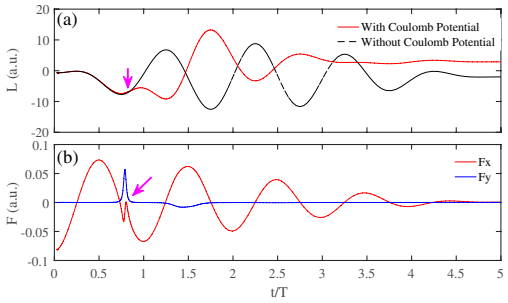

Fig. 6. (a) The evolution of angular momentum of an irregular trajectory (the red curve). In the black curve, we have artificially turned off the Coulomb force. (b) The force along the x and y axes felt by the electron.

trajectory with (red) Coulomb potential. Obviously, the Coulomb force changes the final direction of the angular momentum.

Figure 6 indicates that the angular momentum of the irregular events has been strongly affected by the Coulomb force when the electron returns to the parent ion. In Fig. 7 we show the minimum distance between the parent ion and electron during recollision. The distribution shows a most pronounced peak at around $t = 0.75\,T$–T, which corresponds to when the electron returns to the parent ion for the first time. There are also some other populations locating around $t = T$–$1.25\,T$ and $t = 1.75\,T$–$2\,T$ in Fig. 7. These correspond to when the electron returns to the parent ion for the second and third times, respectively. It is shown that the distance between the electron and ion can be as less as 2.5 a.u., and thus the Coulomb force is very important during the rescattering. This "hard" rescattering makes the final angular momentum exhibit the irregular behavior on the initial transverse momentum.

In conclusion, we have studied the angular momentum of the FTI events. We trace the initial tunneling coordinates and show that the angular momentum distribution depends sensitively on the tunneling time and transverse momentum. For the events, tunneling ionization occurs just before the peak of the laser pulse, and the final angular momentum distribution exhibits a strong correlation with the initial transverse momentum at tunneling. For these events, the final angular momenta are dominantly

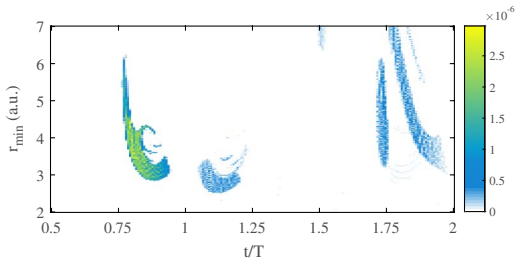

Fig. 7. Minimum distance between the recaptured electron and parent ion during the recollision for the irregular events. The colorbar on the right represents the recapture probability.

determined by the laser fields. This type of FTI takes the dominant part of the FTI events. For the ionization after the peak of the electric fields, the electron could return to parent ion during the laser cycle and lead to a relatively harder rescattering. Because of this rescattering, the final angular momentum lost the correlation with the initial transverse momentum. It suggests that we can control the angular momentum of the FTI events with controllable laser fields (for example, two-color fields[47]).

This work was supported by the National Natural Science Foundation of China (Nos. 11622431 and 61405064).

References

1. M. Lewenstein, P. Balcou, M. Y. Ivanov, A. L'Huillier, and P. B. Corkum, Phys. Rev. A **49**, 2117 (1994).
2. F. Krausz and M. Ivanov, Rev. Mod. Phys. **81**, 163 (2009).
3. C. Zhai, X. Zhang, X. Zhu, L. He, Y. Zhang, B. Wang, Q. Zhang, P. Lan, and P. Lu, Opt. Express **26**, 2775 (2018).
4. L. Xi, X. Zhu, P. Lan, X. Zhang, D. Wang, Q. Zhang, and P. Lu, Phys. Rev. A **95**, 063419 (2017).
5. J. Tan, Y. Li, Y. Zhou, M. He, Y. Chen, M. Li, and P. Lu, Opt. Quantum Electron. **50**, 57 (2018).
6. G. G. Paulus, W. Nicklich, H. Xu, P. Lambropoulos, and H. Walther, Phys. Rev. Lett. **72**, 2851 (1994).
7. M. He, Y. Zhou, Y. Li, M. Li, and P. Lu, Opt. Quantum Electron. **49**, 232 (2017).
8. M. He, Y. Li, Y. Zhou, M. Li, and P. Lu, Phys. Rev. A **93**, 033406 (2016).
9. B. Walker, B. Sheehy, L. F. DiMauro, P. Agostini, K. J. Schafer, and K. C. Kulander, Phys. Rev. Lett. **73**, 1227 (1994).
10. R. Moshammer, B. Feuerstein, W. Schmitt, A. Dorn, C. D. Schröter, J. Ullrich, H. Rottke, C. Trump, M. Wittmann, G. Korn, K. Hoffmann, and W. Sandner, Phys. Rev. Lett. **84**, 447 (2000).
11. T. Weber, M. Weckenbrock, A. Staudte, L. Spielberger, O. Jagutzki, V. Mergel, F. Afaneh, G. Urbasch, M. Vollmer, H. Giessen, and R. Dörner, Phys. Rev. Lett. **84**, 443 (2000).
12. W. Becker, X. Liu, P. J. Ho, and J. H. Eberly, Rev. Mod. Phys. **84**, 1011 (2012).
13. T. Weber, H. Giessen, M. Weckenbrock, G. Urbasch, A. Staudte, L. Spielberger, O. Jagutzki, V. Mergel, M. Vollmer, and R. Dörner, Nature **405**, 658 (2000).
14. X. Ma, Y. Zhou, and P. Lu, Phys. Rev. A **93**, 013425 (2016).
15. D. Ye, M. Li, L. Fu, J. Liu, Q. Gong, Y. Liu, and J. Ullrich, Phys. Rev. Lett. **115**, 123001 (2015).
16. Y. Zhou, C. Huang, Q. Liao, and P. Lu, Phys. Rev. Lett. **109**, 053004 (2012).
17. Y. Zhou, Q. Liao, P. Lan, and P. Lu, Chin. Phys. Lett. **25**, 3995 (2008).
18. Y. Chen, Y. Zhou, Y. Li, M. Li, P. Lan, and P. Lu, Phys. Rev. A **97**, 013428 (2018).
19. P. B. Corkum, Phys. Rev. Lett. **71**, 1994 (1993).
20. R. R. Jones, D. W. Schumacher, and P. H. Bucksbaum, Phys. Rev. A **47**, R49 (1993).
21. L. V. Keldysh, Sov. Phys. JETP **20**, 1307 (1965).
22. Q. Li, X. Tong, T. Morishita, C. Jin, H. Wei, and C. D. Lin, J. Phys. B **47**, 204019 (2014).
23. T. Nubbemeyer, K. Gorling, A. Saenz, U. Eichmann, and W. Sandner, Phys. Rev. Lett. **101**, 233001 (2008).
24. S. Eilzer and U. Eichmann, J. Phys. B **47**, 204014 (2014).
25. H. Zimmermann and U. Eichmann, Phys. Scr. **91**, 104002 (2016).
26. U. Eichmann, T. Nubbemeyer, H. Rottke, and W. Sandner, Nature **461**, 1261 (2009).
27. B. Manschwetus, T. Nubbemeyer, K. Gorling, G. Steinmeyer, U. Eichmann, H. Rottke, and W. Sandner, Phys. Rev. Lett. **102**, 113002 (2009).
28. T. Nubbemeyer, U. Eichmann, and W. Sandner, J. Phys. B **42**, 134010 (2009).
29. J. McKenna, S. Zeng, J. J. Hua, A. M. Sayler, M. Zohrabi, N. G. Johnson, B. Gaire, K. D. Carnes, B. D. Esry, and I. Ben-Itzhak, Phys. Rev. A **84**, 043425 (2011).
30. J. McKenna, A. M. Sayler, B. Gaire, N. G. Kling, B. D. Esry, K. D. Carnes, and I. Ben-Itzhak, New J. Phys. **14**, 103029 (2012).
31. J. Wu, A. Vredenborg, B. Ulrich, L. P. H. Schmidt, M. Meckel, S. Voss, H. Sann, H. Kim, T. Jahnke, and R. Dörner, Phys. Rev. Lett. **107**, 043003 (2011).
32. A. von Veltheim, B. Manschwetus, W. Quan, B. Borchers, G. Steinmeyer, H. Rottke, and W. Sandner, Phys. Rev. Lett. **110**, 023001 (2013).
33. H. Xu, R. Li, and S. L. Chin, Chin. Opt. Lett. **13**, 070007 (2015)
34. T. Peyronel, O. Firstenberg, Q. Liang, S. Hofferberth, A. V. Gorshkov, T. Pohl, M. D. Lukin, and V. Vuletić, Nature **488**, 57 (2012).
35. J. McKenna, S. Zeng, J. J. Hua, A. M. Sayler, M. Zohrabi, N. G. Johnson, B. Gaire, K. D. Carnes, B. D. Esry, and I. Ben-Itzhak, Phys. Rev. A **84**, 043425 (2011).
36. S. Baur, D. Tiarks, G. Rempe, and S. Dürr, Phys. Rev. Lett. **112**, 073901 (2014).
37. D. Paredes-Barato and C. S. Adams, Phys. Rev. Lett. **112**, 040501 (2014).
38. C. Guerlin, J. Bernu, S. Deléglise, C. Sayrin, S. Gleyzes, S. Kuhr, M. Brune, J. M. Raimond, and S. Haroche, Nature **448**, 889 (2007).
39. C. Sayrin, I. Dotsenko, X. Zhou, B. Peaudecerf, T. Rybarczyk, S. Gleyzes, P. Rouchon, M. Mirrahimi, H. Amini, M. Brune, J. M. Raimond, and S. Haroche, Nature **477**, 73 (2011).
40. P. Ge and Y. Liu, J. Phys. B **50**, 125001 (2017).
41. M. V. Ammosov, N. B. Delone, and V. P. Krainov, Sov. Phys. JETP **64**, 1191 (1986).
42. N. B. Delone and V. P. Krainov, J. Opt. Soc. Am. B **8**, 1207 (1991).
43. T. F. Gallagher, Phys. Rev. Lett. **61**, 2304 (1988).
44. P. B. Corkum, N. H. Burnett, and F. Brunel, Phys. Rev. Lett. **62**, 1259 (1989).
45. K. J. Schafer, B. Yang, L. F. DiMauro, and K. C. Kulander, Phys. Rev. Lett. **70**, 1599 (1993).
46. P. B. Corkum, Phys. Rev. Lett. **71**, 1994 (1993).
47. H. Du and N. Yang, Chin. Opt. Lett. **11**, 063202 (2013).